PNAS RESEARCH ARTICLE | APPLIED PHYSICAL SCIENCES OPEN ACCESS

Geometrically modulated contact forces enable hula hoop levitation

Xintong Zhu[a], Olivia Pomerenk[a], and Leif Ristroph[a,1]

Edited by David Weitz, Harvard University, Cambridge, MA; received June 10, 2024; accepted November 4, 2024

Mechanical systems with moving points of contact—including rolling, sliding, and impacts—are common in engineering applications and everyday experiences. The challenges in analyzing such systems are compounded when an object dynamically explores the complex surface shape of a moving structure, as arises in familiar but poorly understood contexts such as hula hooping. We study this activity as a unique form of mechanical levitation against gravity and identify the conditions required for the stable suspension of an object rolling around a gyrating body. We combine robotic experiments involving hoops twirling on surfaces of various geometries and a model that links the motions and shape to the contact forces generated. The in-plane motions of the hoop involve synchronization to the body gyration that is shown to require damping and sufficiently high launching speed. Further, vertical equilibrium is achieved only for bodies with "hips" or a critical slope of the surface, while stability requires an hourglass shape with a "waist" and whose curvature exceeds a critical value. Analysis of the model reveals dimensionless factors that successfully organize and unify observations across a wide range of geometries and kinematics. By revealing and explaining the mechanics of hula hoop levitation, these results motivate strategies for motion control via geometry-dependent contact forces and for accurately predicting the resulting equilibria and their stability.

contact forces | rigid-body dynamics | dynamical systems | parametric excitation | equilibrium and stability

Seemingly simple toys and games often involve surprisingly subtle physics and mathematics (1–4). A prime example from classical mechanics is the spinning top as related to three-dimensional (3D) rotations of rigid bodies and complex couplings between different degrees of freedom, as well as noninertial reference frames and fictitious forces (5). Hula hooping involves these issues and others associated with the rolling point of contact on the body surface, which itself is actuated with gyration motions and whose geometry is expected to strongly affect the hoop dynamics (6, 7). Hence, this familiar playtime activity can serve as an archetype of the challenging class of problems involving parametric excitation by driven supports (6–9) and the mechanics of dynamic contact points with frictional and normal forces (10–13). Such issues are fundamental to related robotic applications for controlled positioning, transforming motions, and harvesting energy from vibrations (14–17).

The physics of hula hooping was first studied as an excitation phenomenon soon after the toy became a fad (6), and more recent interest (8, 18, 19) has come during its renewed popularity as a form of exercise and performance art (20–22). The challenges presented by the 3D problem have restricted previous studies to consider idealized planar or 2D settings without gravity that pertain to an extended mass freely hinged to an oscillating support (6, 7, 23) or a ring rolling around a moving circle (8, 18, 19). Rich dynamics are displayed even within such simplified systems, including a multiplicity of motions for the case of a ring on a circle (8, 18).

While 2D settings can provide insights into planar twirling, they leave unaddressed such basic issues as how a hoop remains suspended against gravity. Weight support is not a goal of the classical analysis of tops and related rotational systems, but it is fundamental to hula hooping and related applications (14–17). At issue is how equilibrium and stability are determined for a free object whose dynamic point of contact can explore the potentially complex surface geometry of an actuated structure. Here, we aim to determine the necessary conditions for levitation through experiments on robotic hula hoopers and models that relate contact forces to the shapes and motions of the hoop and body. This relatable and concrete context also provides the opportunity to understand more general issues involving the geometric modulation of forces on moving contacts and how these

Significance

This study explains the physics and mathematics of how and why a hula hoop can be suspended against gravity. We identify this activity as an example of a more general form of mechanical levitation maintained by rolling points of contact and which depends strongly on body shape. Specifically, we use robotic experiments to show that keeping a hoop at a level requires a sloped surface with "hips" and a curvy "waist," and we present dynamical models that explain our observations and generalize to different shapes and motions. In addition to explaining a familiar but poorly understood activity, our findings may inspire and inform robotic applications for transforming motions, extracting energy from vibrations, and controlling and manipulating objects without gripping.

Author affiliations: [a]Applied Mathematics Laboratory, Courant Institute of Mathematical Sciences, Department of Mathematics, New York University, New York, NY 10012

Author contributions: X.Z. and L.R. designed research; X.Z., O.P., and L.R. performed research; X.Z., O.P., and L.R. analyzed data; and X.Z., O.P., and L.R. wrote the paper.

The authors declare no competing interest.

This article is a PNAS Direct Submission.

[1]To whom correspondence may be addressed. Email: ristroph@cims.nyu.edu.

This article contains supporting information online at https://www.pnas.org/lookup/suppl/doi:10.1073/pnas.2411588121/-/DCSupplemental.

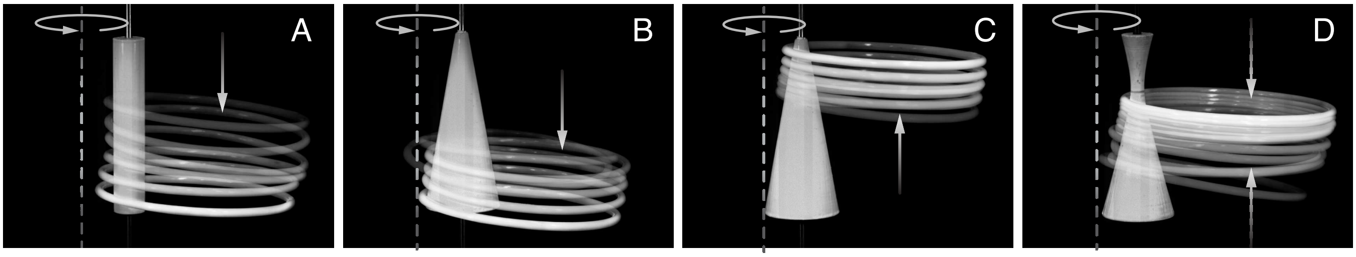

Fig. 1. Vertical motions of hoops on robotic gyrators of different shapes. In all cases, the body motion is circular gyration of radius $R_G = 1$ cm, and the hoop has radius $R_H = 7.4$ cm and mass $M = 15.6$ g. Images from high-speed video are overlaid frames selected every 6 gyration cycles. (*A*) The hoop descends on a cylindrical body of radius 1 cm and gyration frequency $f = \omega/2\pi = 9$ Hz. (*B* and *C*) A hoop on a cone (half-angle 10° and $f = 6$ Hz) ascends or descends depending on its initial height upon release. (*D*) Stable levitation on a hyperboloid (asymptotic half-angle 15°, waist radius 0.5 cm, and $f = 5$ Hz).

might be exploited to induce motions, position, stably suspend, or otherwise manipulate objects.

Robotic Experiments and Motion Tracking

Our experimental apparatus consists of bodies of prescribed shape that are driven with prescribed motions and on which a hoop is released. We consider rigid, axisymmetric bodies formed as surfaces of revolution about the vertical axis and which are manufactured by 3D printing. The surface is rubberized to achieve high friction with a thin, rigid hoop made of plastic. A vertical shaft running through the central axis of the body connects to a motor via appropriate hardware in order to realize gyration, a term used here to mean purely translational revolution of the body in a closed trajectory and without any rotation or spin about its axis. The hoop is launched by hand, and the resulting motions while in contact with the body are recorded by high-speed videography and quantified with custom motion tracking algorithms.

We first ask whether levitation of the hoop can be achieved by simple body shapes. Shown in Fig. 1*A* is the case of a circular cylinder that is driven in circular gyration in which the vertical axis sweeps out a circular cylinder. Selected images from video are overlaid to show the gradual descent of the hoop. The faster orbiting motions of the hoop around the body can be seen in Movies S1–S3 for this and other representative cases, including various forms of conical gyration in which the central axis of the body sweeps out a cone. All trials with a cylindrical body fail to suspend the hoop. The further tests of Fig. 1 *B* and *C* for a conical body in circular gyration reveal the surprising outcome that the hoop may descend or ascend depending on its initial height at release (Movies S4 and S5). The hoop sinks if set free from a low point on the body and rises if released sufficiently high, but it never keeps a level.

These failed attempts using shapes and motions that vary linearly in height motivate more complex geometries. Fig. 1*D* shows that an hourglass-shaped body of hyperboloidal form successfully suspends the hoop. Shown is a case in which the hoop is released low on the body and thereafter rises up to a height just below the "waist" or narrowest point. Movies S6 and S7 show robust trapping for different release locations either above or below the waist.

To better characterize these results, we compare the dynamics on conical and hyperboloidal bodies as representative examples of failed and successful hula hooping. As shown in Movie S8, overhead and side views of the hoop and body allow for temporally and spatially resolved motion tracking. The schematics of Fig. 2 *A* and *B* define the key quantities, and the data are compiled in Fig. 3. The movements of the hoop after being launched by hand are initially somewhat erratic but later show regularity. Notably, the vertical translations of Fig. 1 are corroborated by time-series measurements of the height z of the hoop. As shown for six trials on a conical body in Fig. 3*A*, the hoop descends if released low and ascends if released higher. These motions are reminiscent of an unstable equilibrium point in the vertical dynamics (24). The case of a hyperboloid is shown in Fig. 3*D*. Following release from different heights, the hoop ascends or descends to arrive at a final location below the waist ($z = 0$). These motions are consistent with a stable equilibrium.

Three-dimensional aspects include a slight angle for the plane of the hoop, which is supported at its contact point while sagging under gravity and being slung outward by centrifugal action. The sag angle σ measured relative to the horizontal is plotted in Fig. 3 *B* and *E*, where small values are attained after transient fluctuations.

The in-plane motions consist of twirling in which the hoop center orbits around the body while maintaining continuous contact by rolling without slipping (8, 18). The hoop orbits in the same sense as the body gyration, which is termed direct twirling. Further, our measurements document a synchronization phenomenon in which the orbits of the hoop and body eventually converge toward a state in which the gyration, body, and hoop centers are nearly colinear throughout the cycle and with the contact point on the inner side of the body and the hoop center located outward of the body relative to the gyration center. This direct outward twirling state is defined by the deviation angle δ (Fig. 2*B*) being small in value and nearly constant in time. The time-series data of Fig. 3 *C* and *F* show that, for both body shapes and over repeated trials, initially large oscillations in $\delta(t)$

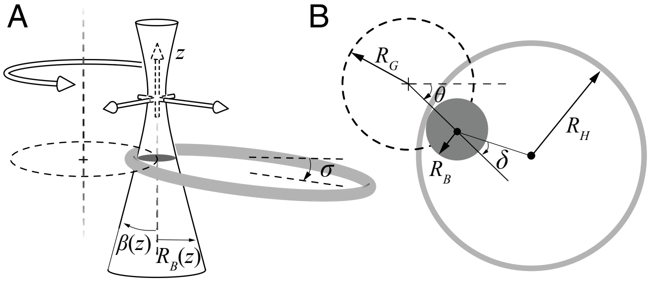

Fig. 2. Schematics and definitions. (*A*) An axisymmetric body is defined by the shape function $R_B(z)$ whose slope determines the local tangent angle $\beta(z)$ of the surface. The hoop center has height z, and its plane forms a sag angle σ with the horizontal. (*B*) The body gyrates around a circle of radius R_G, where $\theta = \omega t$ defines the prescribed motion of the body center. The hoop has radius R_H, and its in-plane location is described by the angle δ of deviation from direct outward twirling, which is the unique state in which the hoop center remains directly outward throughout the gyration cycle.

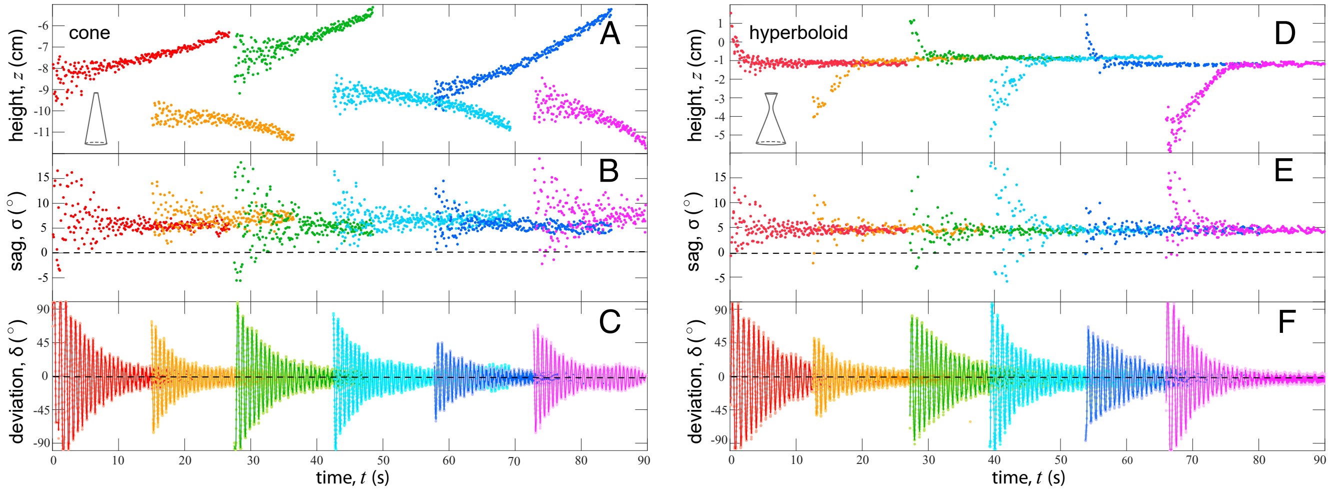

Fig. 3. Measured motions of hoops on a cone (*A*–*C*) and hyperboloid (*D*–*F*). Six trials for each body are shown in different colors. Hoops exit the cone by either climbing or descending whereas stable trapping at a height just below the waist is seen for the hyperboloid. Small sag angles σ and small deviation angles δ at later times are observed for both body types. The body shapes are defined by $R_B^2(z) = R_0^2 + (z \tan \alpha)^2$, where the waist radius is $R_0 = 0$ and 0.5 cm for the cone and hyperboloid, respectively, and the (asymptotic) half-angles are $\alpha = 10°$ and 15°. Here, $R_G = 1$ cm, $f = 5.5$ Hz, $R_H = 7.4$ cm, and $M = 15.6$ g.

gradually decay away to small values. These results suggest that direct outward twirling is an attractor of the planar dynamics, which corroborates a recent hypothesis (19). Our observations counter the more common depiction of hula hooping as inward twirling (8, 18, 25), i.e. with the hoop center located inward of the body center and the contact point on the outside of the body.

Model of 2D Twirling Dynamics

To explain the experimental observations, we first consider a two-dimensional (2D) model of a thin ring twirling around a circular body that is driven to gyrate about a prescribed trajectory. Such a setting has been considered previously as relating to hula hoop dynamics in the horizontal plane (8, 18). The goal of our analysis is to determine whether and for what conditions the hoop synchronizes to the body gyrations. As such, we derive an Euler–Lagrange description of the hoop dynamics, with the key steps summarized here and complete details provided as *Materials and Methods*. We assume that the hoop maintains a single point of contact with the body, which dictates the choice of dynamical variables, and that it rolls without slipping, which appears as a constraint arising from high friction against sliding. The dynamical system of equations is derived from kinetic energy relations with dissipation included via a model for rolling resistance. We explore the predictions of the model by carrying out numerical simulations for conditions relevant to the experiments.

For the dissipationless case without rolling resistance, the model predicts five distinct outcomes for the hoop motion which may be reached for different initial conditions: steady twirling, oscillatory motions, overtwirling, antitwirling, and failure. Failures are identified as those trials that at any time lead to the normal component of the contact force on the hoop reaching or crossing zero, a condition that can be interpreted as loss of contact with the body. The cartoons of Fig. 4*A* illustrate the remaining four states in a frame that rotates with angular speed ω so that the body remains fixed, and the hoop dynamics relative to the body can be assessed by $\delta(t)$. Steady states have constant δ, and an example is direct outward twirling with $\delta(t) = 0$ which is displayed in Fig. 4*B* as a dashed blue line. This state is animated in Movie S9. Oscillatory states involve persistent oscillations of δ (dashed cyan curve) for which the hoop swings back and forth without looping around the body (Movie S10). Overtwirling and antitwirling states involve the unbounded increase or decrease of $\delta(t)$ for which the hoop continually loops around the body in one sense or the other. Examples of each are the pink and purple curves shown in (*B*) with an expanded vertical scale (right axis) and also in Movies S11 and S12.

The map of Fig. 4*C* summarizes the outcomes reached across different initial conditions. This is constructed by carrying out simulations across values of the initial deviation angle $\delta(0)$ and initial velocity $\dot{\delta}(0)$ and classifying the terminal or long-time behavior. Colored regions denote the set of initial conditions leading to each state. As might be expected, overtwirling (pink) occurs for all sufficiently fast and positive initial velocities, and antitwirling (purple) occurs for fast and negative initial velocities. Failures (white) occur for weak launches, which correspond to $\dot{\delta}/\omega \approx -1$ as the body frame speed. An eye-shaped region of oscillatory states (cyan) is centered on direct outward twirling (DOT), which is indicated by the filled blue circle at $(\delta, \dot{\delta}) = (0, 0)$. A second steady state is direct inward twirling (DIT), which is the open blue point at $(\pm\pi, 0)$. This state has the contact point on the outside of the body, and it is singular in the sense that infinitesimal deviations in initial conditions yield wildly different motions such as overtwirling, antitwirling, and high-amplitude oscillations. In contrast, perturbations from DOT lead only to small-amplitude oscillations about $\delta = 0$. This structure is consistent with the dynamical systems classification of DOT as a critical point of the center type.

The inclusion of dissipation, even if small, greatly reduces the available modes. The case with rolling resistance is mapped out in Fig. 4*C*, where it can be seen that the mode structure simplifies to a single steady state (blue) that is reached for all sufficiently high initial velocities and failure (white) otherwise. An example showing the dynamics in the approach to this state is shown as the blue curve in Fig. 4*B*, where a launch from some initial conditions leads to decaying oscillations in $\delta(t)$. Movie S13 animates such a case. The system eventually reaches a small constant $\delta(t \to \infty) \approx -4°$ (solid blue line), with the specific value being dependent on system parameters.

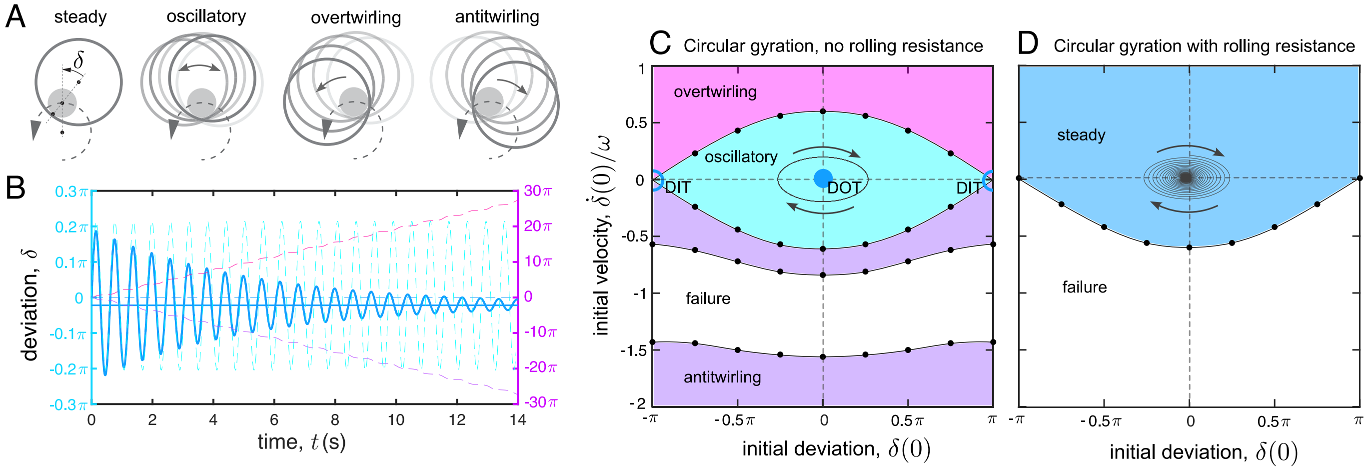

Fig. 4. Twirling modes from a 2D Euler–Lagrange model. (*A*) Classes of solutions for the hoop motions displayed in the body frame. Steady states maintain a fixed posture relative to the body, while oscillatory states involve back-and-forth swings. Over- and antitwirling involve continual looping in the same or opposite sense to gyration. (*B*) Representative outputs of the angular dynamics $\delta(t)$. Without rolling resistance (dashed curves), a steady state with $\delta = 0$ (blue dashed line) arises for isolated initial conditions, and the motions are otherwise oscillatory (cyan), overtwirling (pink), and antitwirling (purple). With rolling resistance (solid curves), a wide variety of initial conditions converge to a common steady state with small $\delta(t \to \infty) = \delta^* < 0$. (*C*) Map of the outcomes (colored regions) across initial conditions for the dissipationless case without rolling resistance. Failures involve a zero crossing of the normal force at some time, which can be interpreted as the hoop losing contact with the body. Direct outward twirling [DOT, $\delta(t) = 0$] and direct inward twirling [DIT, $\delta(t) = \pm\pi$] are isolated steady states. (*D*) Modal map for the case with dissipation via rolling resistance. All sufficiently fast launches lead to decaying oscillations and convergence to a single steady state with equilibrium value δ^*. The parameter values are $f = \omega/2\pi = 5.5$ Hz, $R_G = 1$ cm, $R_H = 7.4$ cm, $M = 15.6$ g, and $R_B = 2$ cm. The rolling resistance coefficient $C_{RR} = 0$ and 0.01 for (*C* and *D*), respectively.

The correspondence with the measurements of Fig. 3 *C* and *F* is striking, suggesting the interpretation that the experiments involve convergence to DOT from the various initial conditions obtained when launching the hoop by hand. Direct outward twirling therefore seems to be the single attractor in the presence of dissipation and one whose basin of attraction extends broadly to all sufficiently fast launches.

Model of 3D Equilibria and Stability

To address the issue of levitation neglected in previous studies, we propose a model that aims to predict the equilibrium and stability of the vertical positioning. Our approach is similar in spirit to that of flight problems in which one is interested in assessing terminal states such as gliding or hovering (26–29), the difference of course being that suspension against gravity is here enabled by solid-on-solid mechanical forces rather than aerodynamics. An outline of the key assumptions and steps is given here, with supporting calculations provided as *Materials and Methods*. We take as a base state direct outward twirling with $\delta = 0$, and the hoop sags at a constant angle σ and makes contact at height z along an axisymmetric body whose shape is defined by the radius function $R_B(z)$. We further assume that the equilibrium is determined by a simple arrangement of forces involving only the hoop weight and the component of the contact force that is directed normally outward from the body surface. A frame moving and rotating with the contact point associates this condition with a balance of the horizontal component of the normal force against the centrifugal force, and the vertical component of the contact force balances weight. Further, torque balance demands that the sag angle match the local slope angle of the body surface, $\sigma = \beta$, where $\tan\beta = -\mathrm{d}R_B/\mathrm{d}z$. These results combine to yield a simple expression for the "lift" or vertical component of the contact force

$$F_V(z) = M\omega^2[R_G - R_B(z) + R_H\cos\beta(z)]\tan\beta(z) \qquad \textbf{[1]}$$

that involves the effective radius for the circular motion of the hoop center about the gyration center. As for hovering flight, equilibrium is achieved for those locations z^* satisfying $F_V(z^*) = Mg$, a condition that involves the body's local radius and slope.

We further extend the flight analogy by associating stability (or instability) with the condition $\mathrm{d}F_V/\mathrm{d}z < 0$ (or > 0), where this so-called stability derivative is to be evaluated at any equilibrium. The analogous criterion is called static stability in flight analyses (26, 29–31). It is motivated by considerations of how the vertical force balance is upset by perturbations away from the equilibrium height, which may be restored or exacerbated depending on the response of F_V due to changes in z. Hence, our model does not treat the full dynamical problem involving all degrees of freedom and their couplings. Rather, the vertical dynamics are viewed as evolving gradually and quasi-statically under the forcing provided by the faster in-plane twirling motions. Similar quasi-steady analyses of the flapping flight of birds and insects evaluate the aerodynamic forces due to fast wing motions and accordingly drive the slower dynamics of the body (28, 31–33).

The model of Eq. **1** explains the observed differences for cones and hyperboloids. A cone has linearly decreasing $R_B(z)$ and constant slope angle β, implying that the normal force and its vertical component $F_V(z)$ increase linearly with height, and a representative curve of the latter is shown in Fig. 5*A*. Any equilibrium proves to be unstable due to the mechanism illustrated in Fig. 5*B*. If placed somewhat above the equilibrium height, then $F_V > Mg$ and the hoop rises. If placed below, then $F_V < Mg$ and the hoop drops. This unstable fixed point is associated with a positive stability derivative $\mathrm{d}F_V/\mathrm{d}z > 0$. Hyperboloidal bodies, on the other hand, have a more intricate $F_V(z)$ profile due to the changing radius and slope (Fig. 5*A*). Equilibria arise as a pair, one of which is unstable and lower on the body and the other stable and higher. The unstable point is like that for the cone. The stable point, however, benefits from the changing slope of the body that leads to a negative stability derivative $\mathrm{d}F_V/\mathrm{d}z < 0$. It remains that $R_B(z)$ decreases, but this effect is overwhelmed by the slope angle $\beta(z)$ decreasing rapidly

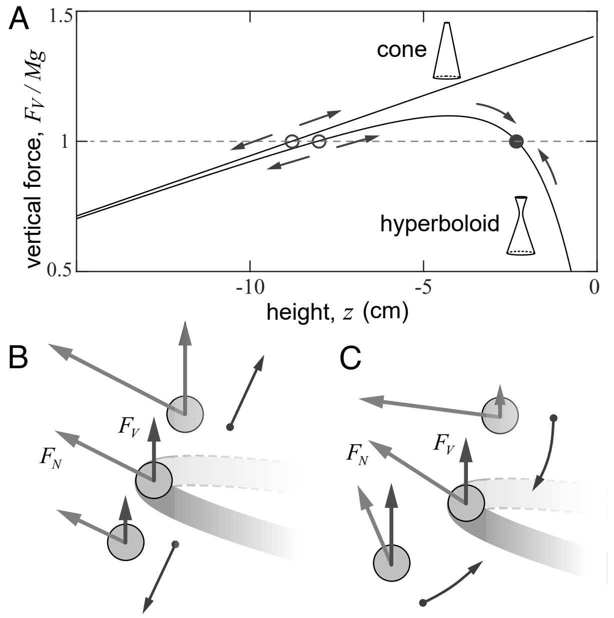

Fig. 5. Model results and stability mechanism. (*A*) Normalized vertical force F_V/Mg as a function of height z for a cone and hyperboloid of $\alpha = 15°$. (*B* and *C*) Unstable and stable fixed points correspond respectively to increasing and decreasing $F_V(z)$.

near the waist and causing $F_V(z)$ to decrease. Hence, as shown in Fig. 5*C*, upward perturbations lead to weaker $F_V < Mg$ that return the hoop toward the equilibrium height, and downward perturbations are restored by $F_V > Mg$.

General Criteria for Levitation and Validation

Further analysis of the model yields general criteria for vertical equilibrium and stability. The equilibrium condition can be recast as

$$S = \frac{\omega^2 \left[R_G - R_B(z^*) + R_H \cos\beta(z^*)\right] \tan\beta(z^*)}{g} = 1, \quad [2]$$

which is the vertical component of the contact force on the hoop normalized by its weight, and where z^* denotes the height attained at equilibrium. The slope factor S can be interpreted as the appropriate nondimensional form of the surface slope that indicates whether the body is sufficiently inclined ($\beta > 0$) to support the hoop against gravity. The criterion explains why cones and hyperboloids ($\beta > 0$) can display behaviors consistent with equilibria, but cylinders ($\beta = 0$ and hence $S = 0$) do not. The formula also indicates that vigorous gyration, i.e., larger R_G and/or higher ω, is beneficial in the sense of permitting smaller slopes. Less intuitive is that a large hoop radius R_H is easier—a fact used by hula hoop instructors when training beginners (34)—but the mass M is inconsequential. [Large R_H and M, however, require large contact forces and thus great effort by the hula hooper, as is evident from record-setting performances for hoop size (35, 36).] The formula also suggests an ideal body shape that is skinny with small radius R_B but with prominent "hips" of large angle β.

Stability of a given equilibrium is dictated by

$$\frac{\mathrm{d}F_V}{\mathrm{d}z} = -\frac{M\omega^2}{\cos^3\beta}\left[-\sin^2\beta\cos\beta + \left(R_G - R_B + R_H\cos^3\beta\right)\kappa\right], \quad [3]$$

where the supporting calculations leading to this result are given as *Materials and Methods*. The formula reveals the importance of the body curvature $\kappa = -(\mathrm{d}\beta/\mathrm{d}z)\cos\beta$ as measured in a vertical section with positive values denoting concavity. The stability condition $\mathrm{d}F_V/\mathrm{d}z < 0$ identifies a critical value of the curvature that must be exceeded to ensure stability: $\kappa > \kappa^* = \sin^2\beta\cos\beta/(R_G - R_B + R_H\cos^3\beta)$. Equivalently, we form the curvature factor $K = \kappa/\kappa^*$ and frame the stability criterion as

$$K = \frac{R_G - R_B(z^*) + R_H\cos^3\beta(z^*)}{\sin^2\beta(z^*)\cos\beta(z^*)}\kappa(z^*) > 1, \quad [4]$$

where the dependencies on z^* are included to highlight the complex ways that the body shape enters. All else being equal, more vigorous gyration with larger R_G promotes stability, as does larger hoop radius R_H. A slender, gently tapering body of small R_B and small β is similarly stabilizing. Crucially, the body cross-section must be concave or hourglass shaped and with a sufficiently curvy "waist," which explains why cones inevitably fail whereas hyperboloids may succeed at stably trapping the hoop.

To quantitatively test these criteria, we conduct further experiments on hyperboloids of different breadths and for varying gyration frequency $f = \omega/2\pi$. For each trial, we measure the terminal equilibrium height z^* attained, and these data are compiled in Fig. 6*A*. The bodies differ in their asymptotic angle $\alpha = \lim_{z\to-\infty}\beta(z)$. For each body shape, we find that there is a critical frequency below which the hoop cannot be suspended at any location, and there is a critical location below which the hoop cannot be suspended for any frequency. To explain these observations, we interrogate the model and plot in Fig. 6*A* the predicted equilibria as curves in the space of (f, z^*). The solid and dashed curves indicate stable and unstable solutions, respectively. The stable solutions of the model capture the general trends in the experimental data, whose errors in f and z^* are shown as bars that are typically smaller than the marker. The model therefore explains the form of the data by identifying for each shape a critical point (marked with a cross) whose value of f must be exceeded to ensure equilibrium and whose value of z^* must be exceeded to ensure stability.

The identified slope and curvature factors provide a universal means for organizing the experimental observations and interpreting the outcomes as stable equilibria. In Fig. 6*B*, the same data are plotted in the space S and K, whose values and error bars can be assessed via Eqs. **2** and **4** using the measured values of z and the imposed values of f and given the prescribed body geometries (see *Materials and Methods*). Stable equilibria are predicted to yield $S = 1$ and $K > 1$, which are highlighted with dashed lines. Indeed, these factors unify the experimental measurements across different shapes and motions by collapsing the data together along the predicted region, which takes the form of vertical stripe in the space of (S, K). The mean and SD $\overline{S} = 1.1 \pm 0.1$ show that the experimental data are slightly greater than the theoretical expectation, and the same discrepancy shows up in Fig. 6*A* as the measured values of z^* being somewhat less than predicted. The discrepancy may be attributed to the model idealizations, e.g. infinitesimal ring thickness, perfect outward twirling with $\delta = 0$, and the neglect of friction in the force balance at equilibrium. Nonetheless, the strong overall correspondence can be taken as evidence that the model accounts well for the geometry-dependent contact forces that give rise to stable levitation.

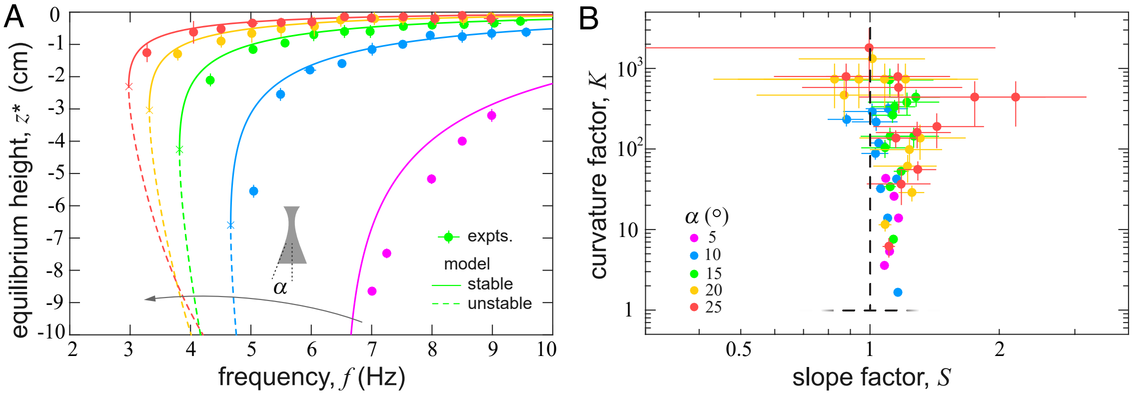

Fig. 6. Comparing model and experiment. (*A*) Trapping height z^* on hyperboloids of varying asymptotic angles α driven with varying $f = \omega/2\pi$ and fixed $R_G = 1$ cm. Experimental data include bars indicating errors that are typically smaller than the marker. Stable and unstable equilibrium solutions of the model are the solid and dashed curves, respectively. (*B*) The data support the predicted slope $S = 1$ and curvature $K > 1$ criteria for equilibrium and stability. The propagated errors may be large for large f and α since the hoop resides very near the waist where the slope and curvature vary rapidly with z.

Discussion and Conclusions

These results reveal two forms of equilibration that give rise to steady-state hula hooping. One is a synchronization process causing the hoop to twirl at the gyration frequency and with its center directed outward of the gyration center. This outcome is dominated by in-plane effects and well captured by 2D modeling. The essential physical requirement is that the hoop be launched sufficiently fast in the same direction as gyration, after which the outward pull by centrifugal action and damping from rolling resistance lead to stable twirling. The second process pertains to the hoop's vertical positioning, which is intrinsically 3D and proves to be strongly dependent on the body profile shape. In particular, our findings identify a necessary "body type" for stable hooping that includes an appropriately angled or sloped surface—i.e., with "hips"—as well as an hourglass-shaped profile with a sufficiently curvy "waist." These aspects are captured by slope and curvature criteria that include the local geometry of the body, the physical properties of the hoop, and the gyration parameters. If only the first condition is met, then the hoop can be supported but will succumb to any perturbation by climbing or falling away. If both conditions are met, the hoop stably keeps a level. These results explain hula hooping as a mechanical levitation phenomenon. More generally, they show how the motion and positioning of an object can be controlled through the geometry and kinematics of a surface in which it is in rolling contact.

Our findings suggest interpretations of hooping by humans, who however differ from our robotic system with respect to body geometry, deformability, and actuation. Humans have noncircular cross-sectional shapes and employ noncircular gyration orbits, both of which are expected to induce unsteady contact forces. The latter case is assessed as *Materials and Methods* via an extension of our 2D model, and the observed weak effects on the twirling mode map and time-averaged normal forces suggest hula hooping dynamics is robust to such factors. A first frustration faced by novices is how to launch the hoop to initiate twirling (34), and our experiments similarly involve false starts in which the hoop loses contact with the body if the launch speed is low. The results of our 2D modeling make sense of these outcomes, and the map of Fig. 4*D* suggests that the best strategy is to start with the hoop and body centers displaced to the same side, i.e. $\delta(0) \approx 0$, and launch at sufficiently high speed in the same direction as gyration, i.e. $\dot{\delta}(0) \gtrsim 0$. If successfully initiated, vertical stabilization can then be achieved via the hips and waist conditions, which should be understood as applicable generally to sloped and curved anatomy and therefore explain twirling on the neck, ankles, wrists, and other hourglass-shaped body parts (37, 38). The resulting passive stability seems essential for understanding how advanced practitioners simultaneously suspend many hoops distributed across the torso and extremities (39). The criteria identified here, being local conditions, permit such multiplicity of stable equilibria.

People are presumably capable of using tactile and visual sensing and motional responses to suspend a hoop even for conditions that are not intrinsically stable. A simple example shows how our results can be extended to such cases of active control. Consider a conical body for which there is generically an unstable equilibrium at height $z^* < 0$. We seek to control the hoop at such a location via a feedback law specifying how the gyration motion is modified according to the hoop height z. The geometric relations $R_B(z) = -z\tan\alpha$ and $\beta(z) = \alpha$ determine via Eq. **1** the vertical force $F_V(z) = M\omega^2[R_G(z) + z\tan\alpha + R_H\cos\alpha]\tan\alpha$ which here includes a control law of the form $R_G(z)$. For example, a linear response $R_G(z) = R_G(z^*) - Cz$ is readily verified to achieve stability $\mathrm{d}F_V/\mathrm{d}z < 0$ so long as $C > \tan\alpha$, where $R_G(z^*)$ is the gyration amplitude at equilibrium. This scheme codifies the intuition that levitation can be accomplished by gyrating less vigorously when the hoop climbs up from z^* and more vigorously when it descends. The same effect may be attained through other laws for $R_G(z)$, $\omega(z)$, and their combination. Ultimately, it is paramount that the condition $\mathrm{d}F_V/\mathrm{d}z < 0$ be satisfied, whether passively or actively.

Our modeling leaves unaddressed many dynamical aspects of the 3D problem. For one, the dual stabilization processes that yield outward twirling and levitation are here analyzed separately but in actuality are concurrent and interactive. Further, it remains to be understood the mechanics of how exactly the hoop climbs or falls, these motions taking the form of helical winding of shallow pitch around the body surface. Explaining such and the 3D dynamics generally will require consideration of all degrees of freedom of the hoop, their governing equations of motions, couplings, and constraints. Air friction may also be considered and may reinforce the effects of rolling resistance. Despite these complexities, our results show that simplified models of the contact forces can effectively predict equilibria and their stability. i.e. whether and where a hoop may eventually levitate. Such knowledge could be useful in applications for moving, manipulating, and positioning objects without gripping (15) and in problems involving dynamic contact points where it may be desirable to geometrically modulate forces.

Materials and Methods

Here, we provide supporting calculations regarding 2D twirling and the 3D model of vertical equilibrium and stability.

Euler–Lagrange Formulation of 2D Twirling. Consider the 2D problem of a thin hoop twirling about a gyrating body of circular shape (8, 18). The schematic of Fig. 7*A* represents an arbitrary configuration at some instant during circular gyration, and our analysis will be shown to be readily modified to account for other body trajectories. Geometric quantities of interest include the radii associated with the hoop R_H, body R_B, and gyration motion R_G. Useful position vectors include the hoop center $\mathbf{r}_H$, the body center $\mathbf{r}_B$, and the contact point $\mathbf{r}_C$ of the hoop on the body surface, all of which are measured relative to the origin at the gyration center. Some useful angles are that of the body center $\theta = \omega t$ as induced by the gyration, the angular location $\phi(t)$ of the contact point around the body surface, and the rotation angle $\psi(t)$ of the hoop about its center. All are measured relative to the x−axis. The normal $\hat{\mathbf{n}} = (\cos\phi, \sin\phi)$ and tangent $\hat{\mathbf{t}} = (-\sin\phi, \cos\phi)$ vectors to the body at the contact point are defined such that the former is directed outward and latter is counterclockwise.

We assume that the hoop always remains in contact with the body, which can be generally formulated as the hoop center lying on a certain circle centered on the body: $|\mathbf{r}_H - \mathbf{r}_B| = R_H - R_B$. As a planar rigid-body dynamics problem, the hoop in principle has three degrees of freedom, e.g. (x_H, y_H, ψ). But by working with the variables (ϕ, ψ), we implicitly assume contact and so the above constraint is met. A second constraint is that the hoop undergoes pure rolling along the body without slipping, which idealizes the effect of strong sliding friction. This can be formulated as a matching of the hoop and body velocities at the contact point:

$$\dot{\mathbf{r}}_B = \dot{\mathbf{r}}_H + \boldsymbol{\omega}_\psi \times (\mathbf{r}_C - \mathbf{r}_H), \qquad [5]$$

where $\boldsymbol{\omega}_\psi = \dot{\psi}\mathbf{k}$ is the angular velocity of the hoop about its center. The above vector constraint can be decomposed into components tangential and normal to the body surface, in which case it can be shown that the normal component is a redundant, weaker form of the contact constraint. The tangential component leads to

$$\psi = \frac{R_H - R_B}{R_H}\phi, \qquad [6]$$

which is readily understood as the "gearing" expected for rolling without slip.

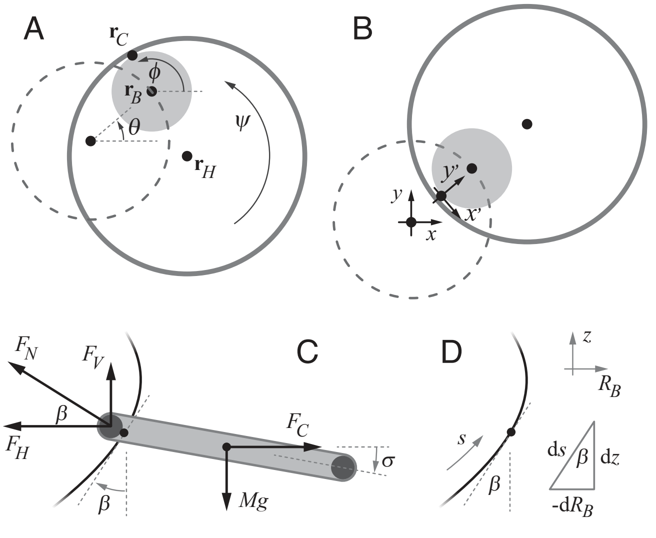

Fig. 7. Schematics and definitions. (*A*) General configuration for the 2D problem of a thin ring in rolling contact with a driven circular body. (*B*) Direct outward twirling has the contact point, body center, and hoop center all colinear with the center of gyration, which is the origin of the lab frame. The hoop is static in the primed frame that follows the contact point and rotates. (*C*) Relevant quantities and forces in a side view of the 3D problem. In the contact point frame, the hoop center is static and the forces balance. (*D*) Geometric quantities relating to the sectional shape of the body.

The constraints can be incorporated into the Euler–Lagrange formulation of the dynamics involving the coordinates (ϕ, ψ). Anticipating that dissipative forces may be of interest, we consider the governing dynamical equations:

$$\begin{aligned} \frac{\partial L}{\partial \phi} - \frac{\mathrm{d}}{\mathrm{d}t}\frac{\partial L}{\partial \dot{\phi}} + \lambda\frac{\partial f}{\partial \phi} - \frac{\partial D}{\partial \dot{\phi}} &= 0 \\ \frac{\partial L}{\partial \psi} - \frac{\mathrm{d}}{\mathrm{d}t}\frac{\partial L}{\partial \dot{\psi}} + \lambda\frac{\partial f}{\partial \psi} - \frac{\partial D}{\partial \dot{\psi}} &= 0 \\ f(\phi, \psi) &= 0. \end{aligned} \qquad [7]$$

The third equation imposes no slip through the constraint function

$$f(\phi, \psi) = \frac{R_H - R_B}{R_H}\phi - \psi, \qquad [8]$$

and the Lagrange multiplier λ is the associated force of constraint whose dynamics is part of the solution. The formulation includes energy loss via nonconservative forces through the Rayleigh dissipation function $D(\phi, \psi, \dot{\phi}, \dot{\psi})$ (40). Below we consider $D = 0$ as appropriate to hooping without dissipation as well as a case in which $D \neq 0$ with a specific form that models the rolling resistance between the hoop and body. The system Eq. **7** constitutes three equations for the three dynamical variables (ϕ, ψ, λ).

The Lagrangian function L has only kinetic energy contributions and therefore takes the form:

$$\begin{aligned} L &= \frac{1}{2}M\dot{x}_H^2 + \frac{1}{2}M\dot{y}_H^2 + \frac{1}{2}I\dot{\psi}^2 \\ &= \frac{1}{2}M\left[-\omega R_G\eta\sin\omega t + (R_H - R_B)\dot{\phi}\sin\phi\right]^2 \\ &\quad + \frac{1}{2}M\left[\omega R_G\cos\omega t - (R_H - R_B)\dot{\phi}\cos\phi\right]^2 \\ &\quad + \frac{1}{2}MR_H^2\dot{\psi}^2. \end{aligned} \qquad [9]$$

The top line is the general form involving translational energy associated with motion of the hoop center and rotational energy due to spin about its center. The expanded form is specific to body motion along an elliptical trajectory, i.e. $R_B(t) = R_G(\eta\cos\omega t, \sin\omega t)$, of which circular gyration with $\eta = 1$ is the base case of interest. While here we restrict our attention to elliptical orbits, the formulation can be readily modified for other types of body motions by differentiating the hoop position: $\mathbf{r}_H = (x_H, y_H) = \mathbf{r}_B - (R_H - R_B)\hat{\mathbf{n}}$.

To assess the effect of dissipation, we consider the specific case of rolling resistance that arises due to material deformation for objects in contact (41). It is typically modeled as a force that resists motion and which is proportional to the normal force:

$$\mathbf{F}_{RR} = -C_{RR}F_N\hat{\mathbf{v}}_{BC}. \qquad [10]$$

Here, C_{RR} is the constant coefficient of rolling resistance that depends on material parameters, and $\mathbf{v}_{BC} = \dot{\mathbf{r}}_{BC} = \dot{\mathbf{r}}_C - \dot{\mathbf{r}}_B = R_B\dot{\phi}\hat{\mathbf{t}}$ is the velocity of the rolling point of contact as seen from a frame centered on the body. The associated Rayleigh dissipation function is determined by the velocity gradient relation:

$$\mathbf{F}_{RR} = -\nabla_{\mathbf{v}_{BC}}D \quad \Rightarrow \quad D = C_{RR}F_N|\mathbf{v}_{BC}|. \qquad [11]$$

This is incorporated into the Euler–Lagrange system of Eq. **7** through the general expression for the normal force in terms of the dynamical variables:

$$\begin{aligned} F_N &= M\mathbf{a}_H \cdot \hat{\mathbf{n}} = M\ddot{\mathbf{r}}_H \cdot \hat{\mathbf{n}} \\ &= M\left[-R_G\omega^2\left(\eta\cos\omega t\cos\phi + \sin\omega t\sin\phi\right) + (R_H - R_B)\dot{\phi}^2\right]. \end{aligned} \qquad [12]$$

Here, we restrict our attention to rolling resistance. Other dissipative effects, such as air drag, could be included individually or in combination by summing dissipation functions similarly derived from models of the nonconservative forces (40).

Numerical Simulations of 2D Twirling, Including Noncircular Orbits. The Euler–Lagrange system of equations is solved numerically using MATLAB's built-in integrator *ode15s*. The initial conditions are specified by $\phi(0)$ and $\dot{\phi}(0)$, from which $\psi(0)$ and $\dot{\psi}(0)$ are determined via the constraint relation Eq. **6**. The numerical solutions for the angle of contact $\phi(t)$ can be recast in terms of $\delta(t) = \phi(t) - \theta(t) + \pi = \phi(t) - \omega t + \pi$, which is the angular position of the hoop center measured in the body frame. The results summarized in Fig. 4 correspond to the following parameter values that are appropriate to circular gyration ($\eta = 1$) and typical of those in experiments: $f = \omega/2\pi = 5.5$ Hz, $R_G = 1$ cm, $R_H = 7.4$ cm, $M = 15.6$ g, and $R_B = 2$ cm. Nonsystematic sweeps through other parameter values show no major qualitative changes in the results. The behavior without and with rolling resistance is compared in Fig. 4 *C* and *D* by comparing coefficient values of $C_{RR} = 0$ and 0.01, the latter typical of rubber in contact with a hard surface, e.g. car tire on road (42). The particular ODE solver *ode15s* was chosen to handle the stiffness of the system that shows up as highly variable dynamics in some regions of parameter space and especially for $C_{RR} = 0$ in the vicinity of DIT reached with the initial conditions $\phi(0) = 0$ and $\dot{\phi}(0) = \omega$.

The outcomes are not markedly affected if the body trajectory is noncircular. Fig. 8 *A* and *B* show maps for elliptical gyration of aspect ratio $\eta = 2$ without and with rolling resistance ($C_{RR} = 0$ and 0.01), respectively. True steady states are absent as expected due to the unsteady forcing from the asymmetric motion. Otherwise, the state-space structures are similar to their circular counterparts. In the case of no rolling resistance shown in (*A*), there are new modes classified as irregular (green) which involve bouts of over- or antitwirling combined with oscillations. With the inclusion of rolling resistance in (*B*), the space simplifies into two outcomes: failures for low-speed or wrong-way launches and an attractor for fast launches that here takes the form of limit-cycle oscillations. These results parallel the circular gyration case of Fig. 4.

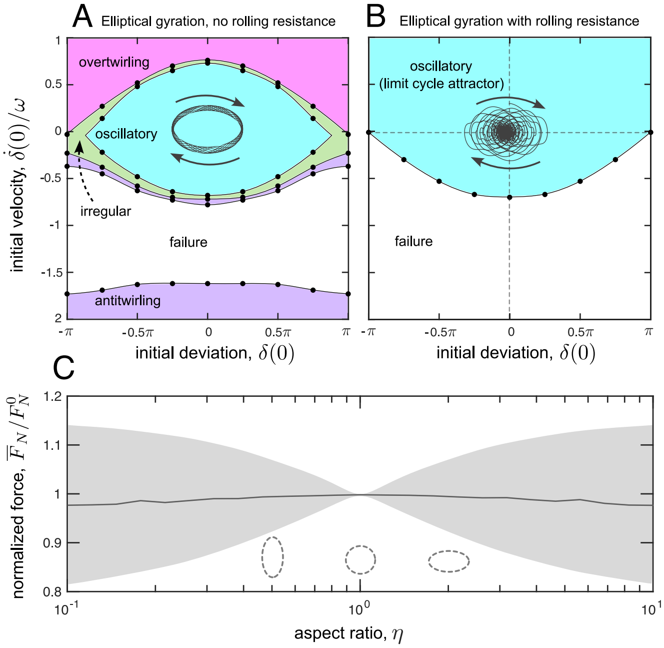

Fig. 8. Numerical solutions to hoop modes and normal force for elliptical gyration. (*A*) Mode map for elliptical body orbit ($\eta = 2$) without rolling resistance ($C_{RR} = 0$). Steady states are absent, and a thin band of irregular motions (green) surrounds the oscillatory modes. An example of oscillatory dynamics $\left(\delta(t), \dot{\delta}(t)\right)$ is shown as the gray curve. (*B*) Mode map with rolling resistance ($C_{RR} = 0.01$). Sufficiently high $\dot{\phi}(0)$ leads to a limit cycle attracting state (cyan region). An example of a converging trajectory is shown in gray. (*C*) The normal force depends weakly on the aspect ratio η of the elliptical gyration orbit. The force $F_N(t)$ is unsteady, and shown are its average value $\overline{F}_N$ at late times (curve) and its range (shaded band). In all cases, we normalize by the steady force F_N^0 produced by DOT for circular gyration at same frequency ω and with an orbit of the same circumferential length.

The normal force, while necessarily unsteady for elliptical orbits, varies little in its mean magnitude as compared to circular gyration. The plot of Fig. 8*C* summarizes the average value (black curve) and range (gray band) of $F_N(t)$ as assessed at late times for elliptical gyration across values of the aspect ratio η and for fixed resistance $C_{RR} = 0.01$. For each value of η, we normalize the force by that of DOT for circular gyration at the same ω and same circumferential length of the gyrational orbit. This ensures the same mean speed of the body motion and thus isolates the effect of the shape of the orbit. The symmetry about $\eta = 1$ reflects the expected equivalence for pairs of ellipses with one as wide as the other is tall. The data show that the mean value differs from the circular case by at most a few percent over widely varying $\eta \in [0.1, 10]$, and the fluctuations in time are typically on the order of 10%.

A further generalization involves noncircular body shapes e.g. ellipses, which might be viewed as more realistically representing the cross-section of human hoopers. Preliminary calculations indicate, however, that the constraint Eq. **5** and in particular its tangential component is nonholonomic and nonintegrable. This presents problems for the Euler–Lagrange formulation (10, 11, 43), and future work in this direction may consider alternative approaches to the dynamics.

Contact Force for Direct Outward Twirling in 2D. For the ideal case of circular gyration and direct outward twirling with $\delta(t) = 0$, the normal force is constant in time. Its dependence on the system parameters is readily derived from the general expression Eq. **12** with $\eta = 1$ and $\delta = \phi - \theta - \pi = 0$ so that $\phi = \theta + \pi = \omega t + \pi$:

$$F_N = M\omega^2(R_G - R_B + R_H). \qquad [13]$$

The same expression can arrived at by considering a reference frame situated on the contact point and rotating with angular frequency ω, in which case the body and hoop do not translate. This is the primed frame shown in Fig. 7*B*. The body and hoop rotate about their respective centers and at rates that lead to no slipping. The general form of the effective force in such a noninertial (accelerating and rotating) frame is

$$\mathbf{F}_r = M\mathbf{a}_r = \mathbf{F} - M\mathbf{A} - M\dot{\mathbf{\Omega}} \times \mathbf{r}_r - M\mathbf{\Omega} \times (\mathbf{\Omega} \times \mathbf{r}_r) - 2M\mathbf{\Omega} \times \mathbf{v}_r \qquad [14]$$

Here, $\mathbf{F}$ denotes the net force in the inertial or lab frame, $\mathbf{A}$ and $\mathbf{\Omega}$ are the translational and rotational accelerations of the moving frame, and $\mathbf{r}_r$, $\mathbf{v}_r$, and $\mathbf{a}_r$ are the position, velocity, and acceleration of the body as seen in the moving frame. The contact point frame has basis vectors: $\mathbf{i}' = (\sin \omega t, -\cos \omega t, 0)$, $\mathbf{j}' = (\cos \omega t, \sin \omega t, 0)$, and $\mathbf{k}' = (0, 0, 1)$. Its translational and rotational accelerations are

$$\begin{aligned} \mathbf{A} &= -\omega^2(R_G - R_B)(\cos \omega t, \sin \omega t, 0) \\ \mathbf{\Omega} &= (0, 0, \omega). \end{aligned} \qquad [15]$$

The force relations greatly simplify since $\dot{\mathbf{\Omega}} = \mathbf{0}$ and $\mathbf{r}_r = R_H\mathbf{j}'$ so that $\mathbf{v}_r = \mathbf{a}_r = \mathbf{F}_r = \mathbf{0}$. Noting that the contact or normal force is the only contributing lab-frame force, one concludes that

$$\mathbf{F} = \mathbf{F}_N = -M\omega^2(R_G - R_B + R_H)(\cos \omega t, \sin \omega t, 0). \qquad [16]$$

This corresponds to a force on the hoop that is directed normally outward from the body surface and whose constant magnitude matches Eq. **13**. From the view of the lab frame, this contact force provides the centripetal acceleration of the mass as it undergoes constant-speed circular motion with an effective radius $R_G - R_B + R_H$. From the view of the contact point frame, the hoop center is still and the normal force at the contact point balances the outward-pointing centrifugal force.

Model of Equilibria in 3D. The 3D problem involves a thin hoop undergoing direct outward twirling at some fixed height along an axisymmetric body. The force diagram relevant to the contact point frame is shown in Fig. 7*C*, where the horizontal component of the normal force at the point of contact balances the centrifugal force, and the vertical component balances the weight of the hoop. This arrangement of forces, which does not include friction, should be taken as a conjecture regarding the factors that dictate the equilibrium. We may define the effective radius $\overline{R}(z) = R_G - R_B(z) + R_H \cos\sigma$, which is modified from its 2D analog to account for the hoop sagging about its contact point by an angle σ and where the dependence on height z indicates how the body shape enters. The horizontal and vertical force balances take the form:

$$\begin{aligned} F_H &= F_N \cos\beta = M\omega^2 \overline{R} \\ F_V &= F_N \sin\beta = Mg. \end{aligned} \qquad [17]$$

Incorporating the first into the second, one arrives at

$$F_V = M\omega^2 \overline{R} \tan\beta = Mg \qquad [18]$$

as the basic expression of the vertical force balance. Further, we demand that torques balance about the point of contact:

$$Mg R_H \cos\sigma = M\omega^2 \overline{R} R_H \sin\sigma. \qquad [19]$$

Combining these results yields

$$\tan\sigma = \frac{Mg}{M\omega^2 \overline{R}} = \tan\beta \qquad [20]$$

and thus $\sigma = \beta$. Therefore, at equilibrium, the hoop sags by an angle equal to that defining the local inclination of the body surface. Given this result, we may eliminate σ in favor of β in defining $\overline{R}(z) = R_G - R_B(z) + R_H \cos\beta(z)$, where the body shape enters through its radius function $R_B(z)$ and the slope angle $\tan\beta(z) = -\mathrm{d}R_B/\mathrm{d}z$. In such case, the vertical force becomes Eq. **1**, and the vertical force balance condition becomes Eq. **2**.

Model of Stability in 3D. Consider an equilibrium away from which the hoop is perturbed in height, thereby perturbing $R_B(z)$ and $\beta(z)$ and upsetting the vertical force balance. We wish to know whether the system responds with a corrective change in height that restores the hoop to the equilibrium, or not. We posit that the hoop ascends if $F_V(z) > Mg$, and it descends if $F_V(z) < Mg$. Since $F_V(z) = Mg$ at equilibrium, it is therefore sufficient to assess the so-called stability derivative $\mathrm{d}F_V/\mathrm{d}z$ at equilibrium, where positive values indicate instability and negative values indicate stability.

The vertical component of the contact force is

$$F_V(z) = M\omega^2 \overline{R}(z) \tan\beta(z) = -M\omega^2 \overline{R}(z) \frac{\mathrm{d}R_B}{\mathrm{d}z}, \qquad [21]$$

where $\overline{R}(z) = R_G - R_B(z) + R_H \cos\beta(z)$ and $\tan\beta(z) = -\mathrm{d}R_B/\mathrm{d}z$. Dropping the dependencies on z, the stability derivative is

$$\begin{aligned} \frac{\mathrm{d}F_V}{\mathrm{d}z} &= -M\omega^2 \left[\left(-\frac{\mathrm{d}R_B}{\mathrm{d}z} - R_H \sin\beta \frac{\mathrm{d}\beta}{\mathrm{d}z} \right) \tan\beta + \overline{R} \frac{\mathrm{d}^2 R_B}{\mathrm{d}z^2} \right] \\ &= -M\omega^2 \left[-(\tan\beta + R_H \kappa \tan\beta) \tan\beta + \frac{\overline{R}\kappa}{\cos^3\beta} \right] \\ &= -M\omega^2 \left[-\tan^2\beta + \left(\frac{\overline{R}}{\cos^3\beta} - R_H \tan^2\beta \right) \kappa \right] \\ &= -\frac{M\omega^2}{\cos^3\beta} \left[-\sin^2\beta \cos\beta + \left(R_G - R_B + R_H \cos^3\beta \right) \kappa \right]. \end{aligned} \qquad [22]$$

This proves Eq. **3**. The simplifications make use of the following geometric relations for the sectional shape of the surface, its slope and curvature, as defined in Fig. 7*D*:

$$\begin{aligned} &\tan\beta = -\frac{\mathrm{d}R_B}{\mathrm{d}z} \quad \text{and} \quad \cos\beta = \frac{\mathrm{d}z}{\mathrm{d}s} \\ &\kappa = -\frac{\mathrm{d}\beta}{\mathrm{d}s} = -\frac{\mathrm{d}\beta}{\mathrm{d}z}\frac{\mathrm{d}z}{\mathrm{d}s} \quad \text{and thus} \quad \frac{\mathrm{d}\beta}{\mathrm{d}z} = -\frac{\kappa}{\cos\beta} \\ &\frac{\mathrm{d}^2 R_B}{\mathrm{d}z^2} = -\sec^2\beta \frac{\mathrm{d}\beta}{\mathrm{d}z} = \frac{\kappa}{\cos^3\beta}. \end{aligned} \qquad [23]$$

The stability condition $\mathrm{d}F_V/\mathrm{d}z < 0$ identifies a critical value for the curvature of the body:

$$\kappa > \kappa* = \frac{\sin^2\beta \cos\beta}{R_G - R_B + R_H \cos^3\beta}. \qquad [24]$$

Equivalently, this relation can be recast in terms of the dimensionless curvature factor K given in Eq. **4**.

Body Geometries and Formulas. Cylindrical, conical, and hyperboloidal surfaces can all be described by the radius function

$$R_B(z) = \sqrt{R_0^2 + (z\tan\alpha)^2}, \qquad [25]$$

where R_0 can be understood as the minimal or waist radius at $z = 0$ and α is the half angle in the limit of $z \to -\infty$. Cylinders are the special case with $R_0 > 0$ and $\alpha = 0$, cones have $R_0 = 0$ and $\alpha > 0$, and hyperboloids have $R_0 > 0$ and $\alpha > 0$. The slope of the body cross-section when viewed from the side is

$$\frac{\mathrm{d}R_B}{\mathrm{d}z} = \frac{z\tan^2\alpha}{\sqrt{R_0^2 + (z\tan\alpha)^2}}, \qquad [26]$$

and the related local slope angle is

$$\tan\beta = -\frac{\mathrm{d}R_B}{\mathrm{d}z} = \frac{-z\tan^2\alpha}{\sqrt{R_0^2 + (z\tan\alpha)^2}}. \qquad [27]$$

One can verify the expected relations that $\tan\beta = 0$ for a cylinder, and $\beta = \alpha$ for the lower half ($z < 0$) of a cone. Hyperboloids have varying angle $\beta(z)$ given by the above formula, from which the expected asymptotic angle relation $\lim_{z\to-\infty} \beta(z) = \alpha$ can be confirmed.

Further, the second derivative is

$$\frac{\mathrm{d}^2 R_B}{\mathrm{d}z^2} = \frac{R_0^2 \tan^2\alpha}{\left[R_0^2 + (z\tan\alpha)^2\right]^{3/2}}. \qquad [28]$$

Using Eq. **23**, the curvature is

$$\kappa = \frac{\mathrm{d}^2 R_B}{\mathrm{d}z^2} \cos^3\beta = \frac{R_0^2 \tan^2\alpha \cos^3\beta}{\left[R_0^2 + (z\tan\alpha)^2\right]^{3/2}}, \qquad [29]$$

as relevant to the side-view cross-section of the body and which is signed such that $\kappa > 0$ for concave or hourglass-shaped surfaces. The expected results that $\kappa = 0$ for cylinders ($\alpha = 0$) and cones ($R_0 = 0$) are readily verified.

The above formulas are used to assess the slope factor S and curvature factor K for our experiments on hyperboloids. That is, for each data marker plotted in Fig. 6*B*, the measured value of z determines $R_B(z)$ via Eq. **25** and $\beta(z)$ via Eq. **27**, and these are input into Eq. **2** to yield the displayed value of S. Similarly, the measured value of z determines $R_B(z)$ via Eq. **25**, $\beta(z)$ via Eq. **27**, and $\kappa(z)$ via Eq. **29**, and all these are input into Eq. **4** to yield the displayed value of K.

Data, Materials, and Software Availability. All study data are included in the article and/or supporting information.

ACKNOWLEDGMENTS. We thank J. Eaton for early work on motion tracking and modeling, and M. Holmes-Cerfon and C. Peskin for useful discussions. We acknowledge support from the U.S. NSF through the grants DMS-1847955 and DMS- 2407787.

1. M. Gardner, Mathematical games. *Sci. Am.* **222**, 132–140 (1970).
2. M. J. Osborne, *An Introduction to Game Theory* (Oxford University Press, 2004).
3. J. Güémez, C. Fiolhais, M. Fiolhais, Toys in physics lectures and demonstrations–A brief review. *Phys. Educ.* **44**, 53 (2009).
4. S. Rajasekar, R. Velusamy, M. A. Sanjuán, *Understanding The Physics Of Toys: Principles, Theory And Exercises* (World Scientific, 2023).
5. S. T. Thornton, J. B. Marion, *Classical Dynamics of Particles and Systems* (Cengage Learning, 2021).
6. T. K. Caughey, Hula-hoop: An example of heteroparametric excitation. *Am. J. Phys.* **28**, 104–109 (1960).
7. J. F. Wilson, Parametric spin resonance for a spinner with an orbiting pivot. *Int. J. Non Linear Mech.* **33**, 189–200 (1998).
8. A. Belyakov, A. Seyranian, The hula-hoop problem. *Dokl. Phys.* **55**, 99–104 (2010).
9. T. Bakri, R. Nabergoj, A. Tondl, F. Verhulst, Parametric excitation in non-linear dynamics. *Int. J. Non Linear Mech.* **39**, 311–329 (2004).
10. J. I. Neimark, N. A. Fafaev, *Dynamics of Nonholonomic Systems* (American Mathematical Soc., 2004), vol. 33.
11. M. Flannery, The enigma of nonholonomic constraints. *Am. J. Phys.* **73**, 265–272 (2005).
12. A. C. Fischer-Cripps, *Introduction to Contact Mechanics* (Springer, 2007), vol. 101.
13. V. L. Popov *et al.*, *Contact Mechanics and Friction* (Springer, 2010).
14. R. Balasubramaniam, M. T. Turvey, Coordination modes in the multisegmental dynamics of hula hooping. *Biol. Cybern.* **90**, 176–190 (2004).
15. A. Bicchi, R Sorrentino, "Dexterous manipulation through rolling" in *Proceedings of 1995 IEEE International Conference on Robotics and Automation* (IEEE, 1995), vol. 1, pp. 452–457.
16. C. Lu, C. Wang, C. Sung, P. C. Chao, Dynamic analysis of a motion transformer mimicking a hula hoop. *J. Vib. Acoust.* **133**, 014501 (2011).
17. C. Lu, Y. Wang, C. Sung, P. C. Chao, A hula-hoop energy-harvesting system. *IEEE Trans. Magn.* **47**, 2395–2398 (2011).
18. A. P. Seyranian, A. O. Belyakov, How to twirl a hula hoop. *Am. J. Phys.* **79**, 712–715 (2011).
19. R. Cross, Physics of a hula hoop. *Phys. Educ.* **56**, 025015 (2021).
20. T. Cluff, D. Robertson, R. Balasubramaniam, Kinetics of hula hooping: An inverse dynamics analysis. *Hum. Mov. Sci.* **27**, 622–635 (2008).
21. S. M. McGill, E. D. Cambridge, J. T. Andersen, A six-week trial of hula hooping using a weighted hoop: Effects on skinfold, girths, weight, and torso muscle endurance. *J. Strength Cond. Res.* **29**, 1279–1284 (2015).
22. A. Garcia-Falgueras *et al.*, Hula hoop in fitness and the centripetal force. *Psychology* **7**, 1503 (2016).
23. T. Horikawa, Motion of hula-hoop and its stability. *Keio Sci. Tech. Rep.* **40**, 27–39 (1987).
24. S. H. Strogatz, *Nonlinear Dynamics and Chaos with Student Solutions Manual: With Applications to Physics, Biology, Chemistry, and Engineering* (CRC Press, 2018).
25. H. Richard Crane, Chattering, the chatterring, and the hula hoop. *Phys. Teach.* **30**, 306–308 (1992).
26. B. Etkin, L. D. Reid, *Dynamics of Flight: Stability and Control* (John Wiley & Sons, 1995).
27. G. Taylor, A. Thomas, Animal flight dynamics II. Longitudinal stability in flapping flight. *J. Theor. Biol.* **214**, 351–370 (2002).
28. M. Sun, Insect flight dynamics: Stability and control. *Rev. Mod. Phys.* **86**, 615 (2014).
29. H. Li, T. Goodwill, Z. J. Wang, L. Ristroph, Centre of mass location, flight modes, stability and dynamic modelling of gliders. *J. Fluid Mech.* **937**, A6 (2022).
30. B. Liu, L. Ristroph, A. Weathers, S. Childress, J. Zhang, Intrinsic stability of a body hovering in an oscillating airflow. *Phys. Rev. Lett.* **108**, 068103 (2012).
31. L. Ristroph *et al.*, Active and passive stabilization of body pitch in insect flight. *J. R. Soc. Interface* **10**, 20130237 (2013).
32. L. Ristroph *et al.*, Discovering the flight autostabilizer of fruit flies by inducing aerial stumbles. *Proc. Natl. Acad. Sci. U.S.A.* **107**, 4820–4824 (2010).
33. L. Ristroph, S. Childress, Stable hovering of a jellyfish-like flying machine. *J. R. Soc. Interface* **11**, 20130992 (2014).
34. J. Coyne, "I taught a total beginner how to hula hoop around the waist first time" (Hoopsmiles, 2019). www.youtube.com/watch?v=2ZLuZh2sF9c. Accessed 1 March 2023.
35. A. Richards, "Largest hula hoop spun - guinness world records day" (Guinness World Records, 2017). www.youtube.com/watch?v=1opbqvh_RTE. Accessed 1 March 2023.
36. A. Richards, "Largest hula hoop spun getti kehayova - guinness world records" (Guinness World Records, 2019). www.youtube.com/watch?v=-74jxaheG7I&t=13s. Accessed 1 March 2023.
37. J. P. Jenack, Neck hooping, National Circus Project. www.youtube.com/watch?v=y5C5N8rAcBI. Accessed 1 March 2023.
38. D. Love, "How to hula hoop on your legs and knees". www.youtube.com/watch?v=9cNRafdR4uE. Accessed 1 March 2023.
39. L. Esner, "Woman spins multiple hula hoops all over her body". www.youtube.com/shorts/-qSt0LHNcxM. Accessed 1 March 2023.
40. A. Maria Bersani, P. Caressa, Lagrangian descriptions of dissipative systems: A review. *Math. Mech. Solids* **26**, 785–803 (2021).
41. G. Komandi, An evaluation of the concept of rolling resistance. *J. Terrramech.* **804**, 159–166 (1999).
42. J. Ejsmont, W. Owczarzak, Engineering method of tire rolling resistance evaluation. *Measurement* **145**, 144–149 (2019).
43. A. M. Bloch, J. E. Marsden, D. V. Zenkov, Nonholonomic dynamics. *Not. AMS* **52**, 320–329 (2005).